Passive Multifrequency Forward-Scatter Radar Measurements of Airborne Targets Using Broadcasting Signals

MICAELA CONTU
ALESSANDRO DE LUCA
STANISLAV HRISTOV
LIAM DANIEL
ANDY STOVE, Senior Member, IEEE
MARINA GASHINOVA
MIKHAIL CHERNIAKOV
University of Birmingham, Birmingham, U.K.

DEBORA PASTINA, Member, IEEE
PIERFRANCESCO LOMBARDO, Member, IEEE
University of Rome "La Sapienza", Rome, Italy

AURORA BARUZZI
DIEGO CRISTALLINI, Member, IEEE
Fraunhofer FHR, Wachtberg, Germany

This paper demonstrates the feasibility and effectiveness of forward-scatter radar (FSR) target detection based on the signals of opportunity made available by standard radio and TV broadcast transmission stations. This passive FSR (P-FSR) operation is obtained by means of a simple and robust correlation process based on self-mixing. This is shown to be very effective in extracting the characteristic FSR modulation produced by airborne targets, from the signals received from frequency modulated, digital audio broadcasting, and digital video broadcasting transmitters of opportunity. Target detectability is discussed as a function of the carrier frequency, the target size, and its height at the baseline crossing. Experimental results are shown using a wide variety of sources of opportunity, target types, baselines, and receiver configurations. The target signatures obtained from the different illuminators are compared and ways of extracting the kinematic parameters of the aircraft are discussed. This validates the claimed effectiveness and robustness of the P-FSR with the presented processing scheme.

Manuscript received April 15, 2016; revised July 22, 2016; released for publication 22, 2016. Date of publication January 27, 2017; date of current version June 7, 2017.

DOI. No. 10.1109/TAES.2017.2649198

Refereeing of this contribution was handled by M. Kaplan.

This work was supported by the U.K. Research Council EPSRC within Projects EP/L024578/1 and EP/J006610/1.

Authors' addresses: M. Contu, A. De Luca, S. Hristov, L. Daniel, A. Stove, M. Gashinova, and M. Cherniakov are with the Department of Electronic, Electrical and Systems Engineering, University of Birmingham, Birmingham B15 2TT, U.K, E-mail: (contumicaela@gmail.com; axd357@bham.ac.uk; sxh909@student.bham.ac.uk; l.y.daniel@bham.ac.uk; a.stove@bham.ac.uk; m.s.gashinova@bham.ac.uk; m.cherniakov@bham.ac.uk); D. Pastina and P. Lombardo are with the DIET Department, University of Rome "La Sapienza", Rome 00184, Italy, E-mail: (debora.pastina@uniroma1.it; pierfrancesco.lombardo@uniroma1.it); A. Baruzzi and D. Cristallini are with the Fraunhofer FHR, Wachtberg 53343, Germany, E-mail: (aurora.baruzzi@fhr.fraunhofer.de; diego.cristallini@fhr.fraunhofer.de).

I. INTRODUCTION

Forward-Scatter radar (FSR) is a subclass of bistatic radar, defined by the bistatic angle (β) close to 180° [1], [2] so that transmitter and receiver are facing each other and the target is close to the line between them. Any systems using forward scattering, thus, approximates to an "electronic fence." As can be seen from the equations for the resolution of a bistatic radar [3], both the range resolution and the Doppler (velocity) resolution become very poor when the forward-scatter case is approached. In this case the "ambiguity diagram" [3] as conventionally understood becomes meaningless. The target can be almost anywhere the range-velocity space, being limited only to remain within the forward-scatter regime throughout the measurement time. It was demonstrated in [4], however, that precise estimates of the target's speed can be obtained by matched filtering the nonconstant Doppler signal seen from a target as it approaches, passes through and emerges from the forward-scattering region.

The behavior of the "known" but nonconstant reference Doppler profile differs from the conventional ambiguity function which assumes a constant Doppler shift but has some analogy with the nonlinear (parabolic) phase response assumed in synthetic aperture radar (SAR) processing. As in the SAR case, this method generates "cross-range" (cross baseline) information, but as the target is known to be moving and the radar stationary, the FSR case yields cross-range speed rather than cross-range position. In practice, in this approach to FSR target detection the Doppler processing is preceded by a conventional "matched filter" in the fast-time domain. Such an approach uses the assumption that for the low Doppler shifts seen in this mode, the signals from the broadcast transmitters can be treated as being Doppler tolerant. This is also analogous to many forms of SAR processing.

The forward-scattering principle for target detection is the interruption of the direct signal between transmitter (Tx) and receiver (Rx) due to the crossing of their line of sight (LoS) [5]. Rather than considering FSR as a "singular" case of a "general" bistatic configuration, it is more useful to see FSR as a separate class of a radar system. This is because the FSR target characteristics originate from different physical principles from most traditional radar. In the forward-scatter case, the target signature is obtained through the shadowing of the direct signal by the target [1], rather than reflections from it. (In practice, this means that only moving targets can be detected since the receiver must look for a change in the level of the direct signal.)

Using broadcasting transmitters as illuminators for passive radars meanings, which have not been designed for radar use, mean that the ambiguity function is not under

the system designer's control. However, this is not an issue in the forward-scatter case because of the "explosion" of the ambiguity function in the forward-scatter case to cover all the range-velocity space. This distinctive feature defines FSR's strengths and limitations at the same time. The physical principle and topology of FSR implies that the target can only be detected when it is moving within the proximity of the baseline. Although the radar has no "classical" resolution in this configuration, the physical principle on which these systems rely allows the detection performance to be completely independent on both the target material and shape [1]. This makes this type of radar a good counter-stealth system, which naturally makes it capable to serve as an electronic fence [6]. As well as giving a return which is independent of the target material, the target FS cross section (FSCS) in the optical scattering region is usually significantly bigger than its monostatic and bistatic counterparts.

As stated in [2], a FSR mode can add considerable extra benefits to the existing bistatic radar and can, in practice, be integrated in those systems without requiring significant changes to the hardware. One of the appealing characteristic of a P-FSR system is that as long as the frequencies of signals of opportunity are within the receiver bandwidth, such signals may be exploited in FSR applications. When multiple baselines are available, crossing time-based techniques can be exploited for the nonambiguous retrieval of all the kinematic parameters [7], [8]. As shown in this paper, the power level is not a restriction in a wide range of situations; thus, only signal frequency has a strong impact on the P-FSR performance. This significantly reduces the constraints on the range of operational waveforms, which will allow such a system to function effectively.

The goal of this paper is twofold. First, it presents initial results of the ongoing research. Second, it demonstrates the feasibility and practical applicability of P-FSR using: digital video broadcasting-terrestrial—DVB-T [9], digital audio broadcasting—DAB [10], and frequency modulated—FM [11] waveforms of opportunity to detect airborne targets and estimate target speed. For this purpose, two challenging scenarios involving small targets and nonideal trajectories (i.e., with crossing angles significantly smaller than 90°) are considered.

The paper is organized as follows. In Section II, a new simple approach to extract Doppler signature from the received signal is presented having its effectiveness analytically demonstrated for both digital (DAB and DVB-T) and analogue (FM) modulated signals in the Appendix. Some considerations about the received power and the influence of the target trajectory on the system performance are then discussed in Section III. Trials scenarios and experimental setups to detect various aircrafts are described in Sections IV and V together with experimental results analysis. Speed estimations for the targets, obtained from the data, are presented in Section VI. At the end of the paper, general conclusions are formulated.

II. FORWARD-SCATTER TARGET DOPPLER SIGNATURE EXTRACTION PROCESSING CHAIN

Optimal radar detection is based on correlation of the received ("surveillance") signal with a sample of the transmitted signal (the "reference" signal). This same approach is used in systems using illuminators of opportunity (IoOs) and in forward-scatter radars and also in the algorithm described here. Systems using IoOs usually have to acquire the reference signal using an antenna steered toward the transmitter. The surveillance signal is often acquired by a separate antenna, which is frequently arranged to have a near null in its pattern in the direction of the transmitter, to avoid overloading from the strong direct signal. The separate reference signal is assumed to be target free. In contrast for the FSR case, the "reference" signal (direct signal) is received in the same channel, as the surveillance signal. The algorithm described in this paper actually exploits this feature of the forward-scatter geometry to operate a self-mixing between these signals.

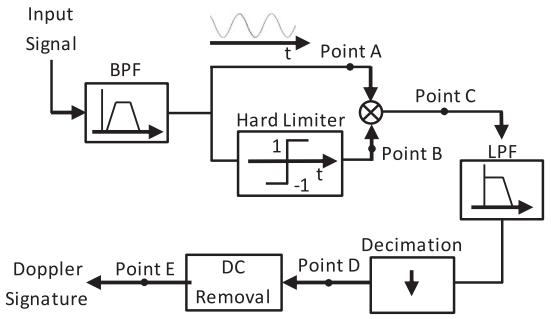

Fig. 1. Algorithm block diagram.

This research has used the algorithm introduced in [12]. The approach is based on the physical operational principle of FSR, which is the amplitude modulation of the direct path (leakage) signal due to target shadowing. Hence, if we manage to extract the amplitude modulation from the detected signal, we will separate the reference signal from the target contribution.

It must be pointed out that the processing scheme considered here needs a direct signal-to-noise ratio (DSNR) at the input to the correlator which is significantly above 0 dB to operate properly [13]. This condition is nearly always satisfied as the broadcasting transmitters can be assumed to guarantee DSNR $\geq$ 10 dB anywhere within their coverage area.

The block diagram of the processing chain used to extract the Doppler signature is shown in Fig. 1. The input to this block diagram is a digital received signal strength indicator signal down converted to an intermediate frequency (IF), which may be a zero IF if quadrature channels are used. Following conventional receiver design practice, this signal is first passed through the band-pass filter (BPF) in order to remove out-of-bands signals and noise, which would otherwise degrade the detection process. Its bandwidth is chosen to match the transmitted signal bandwidth, and in an operational system, it is most easily implemented by using the same filter design as is used by the receivers which the transmitter originally intended.

The output of BPF is split into two channels.

1) The first channel passes the filtered signal as it is (see Fig. 1—Point A).

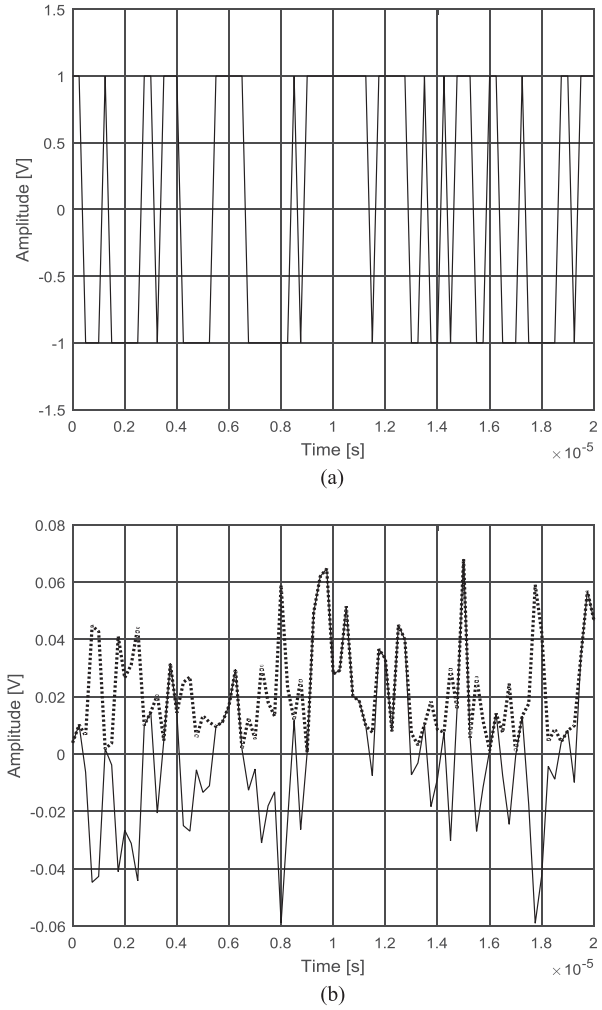

Fig. 2. Hard limiter response. (a) Signal at point A (solid line) and (b) signal at point C (dashed line).

2) The second channel consists of a hard limiter that saturates positive and negative amplitudes values, respectively, to 1 and -1 creating a reference signal without any amplitude modulation. The signal after hard limiter maintains the original signal's phase or frequency information (see Fig. 1—Point B). It is worth nothing that this operation is done without adding extra noise even if the hard limiter is a nonlinear component [14].

In order to extract the target information, the received signal (Point A) is multiplied with the hard-limited reference signal (Point B). It is well known [4] that for a fast oscillating function, the hard-limited version is highly correlated with the original (nonlimited) signal, and, therefore, only minimal loss in the signal processing efficiency is expected from using this scheme.

Fig. 2(a) and (b) shows, respectively, the response of the hard limiter for a general received signal (Point B) and both the signal after the BPF (solid line—Point A) and the signal resulting from the multiplication at point C (dashed line).

Such multiplication when applied to real signals is mathematically equivalent to the extraction of the absolute value of the signal at Point A [15].

The output signal is then low-pass filtered by low-pass filter (LPF) which is designed to leave only frequency components which are within the range of the expected Doppler frequencies from targets which are close to the baseline, as discussed below. The amplitude modulation rate due to passage of the target through the baseline is lower than the range of these Doppler shifts.

If the Doppler shifts are considered only within the main lobe (ML) of the FSCS, then the target speed can be assumed to be constant within such a narrow scattering period and for a linear trajectory, its upper limit [2] is expressed by

$$f_{D,\mathrm{FS}} \leq \frac{v_{tg}\cos(\delta)}{2D} \tag{1}$$

where v_{tg} is the speed and δ is the inclination of target trajectory with respect to the bistatic angle bisector. D is the effective target shadow aperture dimension. In order to estimate the upper limit of the expected Doppler frequency for an airborne target, the value of D in (1) should be taken as the smallest value of either wingspan or body length [2].

If, however, the target FSCS sidelobes are included into the overall forward-scatter Doppler signature, they can potentially deliver richer information to be used for target classification [16]. As with any other type of Doppler radar, the filter design, thus, depends on the scenario and on the range of targets which must be detected.

Thus, for our purpose, higher Doppler shifts than the bare minimum are considered. For instance, in the case of DVB-T signal of opportunity, for a 35-m airliner with a typical cruise speed of 600 km/h, the maximum Doppler frequency $f_{D,\mathrm{FS}}$ within the ML corresponds to orthogonal crossing and is around 2 Hz according to (1). On the other hand, recalling the bistatic Doppler frequency formula $f_D = (2v_{tg}/\lambda)\cos(\delta)\cos(\beta/2)$ [17], where λ is the wavelength of the transmitted signal and considering bistatic angles close to the forward geometry (for instance, taking $\beta = 175°$), the Doppler frequencies would be up to 30 Hz. Thus, considering the Doppler bandwidth to be of order of tens of Hertz, the LPF cutoff frequency is set to 100 Hz for all the considered signals to just exceed minimum required Nyquist criterion. This means that, for instance, if the DVB-T $B = 10$-MHz channel is considered, after the LPF the bandwidth will become $B_2 = 100$ Hz, and a 50-dB signal-to-noise ratio (SNR) gain will be expected (i.e., a noise bandwidth reduction of $B/B_2 = 10^5$ meaning 50-dB less noise power).

The signal obtained at the output of the LPF is the target Doppler signature. The last two blocks of the processing chain consist of the decimation, which reduces signal sample rate in proportion to its effective bandwidth and the cancellation of the dc component. A further processing stage (not explicitly considered here) is the matched filter compression, which may provide us a further integration gain of $B_2(1/T_{\mathrm{int}}) = 1000 \Rightarrow 30$ dB, due to the further bandwidth reduction proportional to the visibility time. Such a visibility time, due to coherency and nonfluctuating targets, in FSR is coincident with the integration time T_{int} (typically around 10 s) since the filter operation is a form of coherent integration.

The final matched filtering with the overall Doppler signature of the target will substantially recover any "loss" due to making the LPF in Fig. 1 wider than necessary, so the design of the latter is not critical to the performance of the system.

The independence of the extracted Doppler signature from the analogue and digital modulations applied to the communication signals is addressed in Appendix.

III. POWER BUDGET ANALYSIS

As stated above the main goal of this work is to investigate the performance of passive FSR for the detection and the estimation of the kinematic parameters of airborne targets. Therefore in this subsection we give our attention to a preliminary estimation of the power budget needed to guarantee the system efficiency.

A. FSCS Patterns

In order to calculate the sensitivity of the system knowledge of the FSCS of the target is required.

The obvious limitation of FSR for air target detection is that the target should come close to the baseline and preferably cross it. This is clearly not strictly possible if both transmitter and receiver are at low altitude. However, as long as the target's main forward-scatter lobe impinges on the receiver, we can expect operation in the FS regime.

1) Analytical Characterization: As is well known, a target illuminated by an electromagnetic wave behaves as a secondary source reradiating energy according to its radiation pattern determined by the RCS. An important parameter which characterizes the extent of the forward-scatter main lobe (FSML) is its −3-dB beamwidth, which is given by [2]

$$\theta_{\mathrm{FSML}} = \lambda / D. \tag{2}$$

Therefore, depending on the target's electrical dimensions, its flight height and the ranges to the transmitter and the receiver, there might be situations when the receiver is not illuminated by the main FS lobe. The widths of the FS ML for a Cessna 172 estimated by both analytical formula (2) and full-wave modeling at frequencies of broadcasting IoOs are given in Table I in Section III-A3. More information for a range of targets and frequencies can be found in [2].

Fig. 3 shows the general FSR situation when an airborne target moves through the area between Tx, at height h_t, and Rx, at height h_r, separated by the baseline L in a flat earth model approximation. This baseline is obtained as the projection of the LoS between Tx and Rx onto the earth's surface.

We assume that the aircraft crosses the vertical plane containing the LoS between transmitter and receiver (the baseline plane) at the altitude h_{PC}, while the LoS height is h_{BC}. The width of the FSML in elevation, θ_{EL}, is given by using (2) with the target vertical dimension being used as the value for D. Since the receiver is within the FSML, even though the target does not strictly cross the baseline, its forward-scatter signature can still be detected.

It is worth noting that the receiver may also capture signals reirradiated within the target side lobes with reduced scattered power. With this in mind, the minimum distance the target has to be from the receiver to be detected can be approximated for low target altitude as (2)

$$d = \frac{h_{\mathrm{PC}} - h_{\mathrm{BC}}}{\tan(\theta_{\mathrm{EL}}/2)} = \frac{\Delta h_C}{\tan(\theta_{\mathrm{EL}}/2)}. \tag{3}$$

In (3), the baseline inclination has been assumed negligible since in most cases, the angle is of the order of fraction of degree.

The peak value of the FSCS is [1]

$$\sigma_{\mathrm{FS\,max}} = 4\pi \frac{A^2}{\lambda^2}. \tag{4}$$

The comparison between (2) and (4) suggests that the choice of the operational frequency is a compromise between having a wide ML and maximizing the peak gain in the forward-scatter direction. In particular, the use of higher frequencies to guarantee a higher power level at the receiver would result in a more stringent constraint on the maximum altitude at which the target can be detected. Multifrequency operation can, thus, deliver enhanced performance in terms of both coverage and SNR. This can be easily achieved by means of passive systems exploiting broadcasting without any effort to build a transmitter able to synthesize such range of frequencies at the same time.

2) Electromagnetic Modeling: Simulation of RCS of a small aircraft, a Cessna 172, has been carried out using CST Microwave Studio [18]. This type of aircraft was modeled since it was used as a test target in some of the experiments (described in Section V-A below). Fig. 4(a) shows the CAD model of the target, and Fig. 4(b) shows the CST model of its RCS at 223 MHz, i.e., a DAB frequency.

The figure also indicates the horizontal plane-wave illumination broad side onto the target plane cut. This corresponds to the baseline plane in Fig. 4 where θ is the elevation angle (defined as negative below horizontal). In order to simulate RCS of aircraft at particular altitude with respect to the transmitter, the angle of illumination was

TABLE I
Simulated (CST) and Analytical (an.) FSCS Results

Parameter of FSCS	93 MHz		223 MHz		650 MHz	
	CST	An.	CST	An.	CST	An.
θ_{EL} [deg]	70.4	79.7	36.9	33.6	13.5	11.5
$\sigma_{\mathrm{FS\,max}}$ [dBm^2]	23.5	23.25	30.43	30.76	38.35	40.1

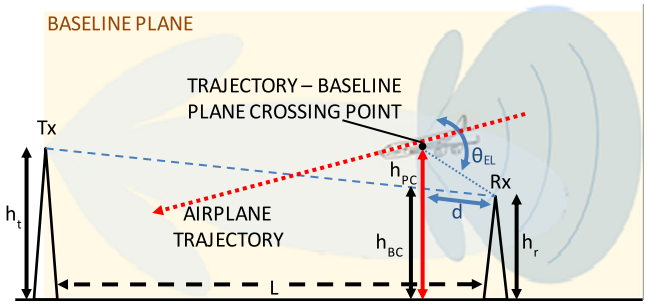

Fig. 3. FSR aircraft crossing geometry: Target minimum distance from the receiver at the crossing.

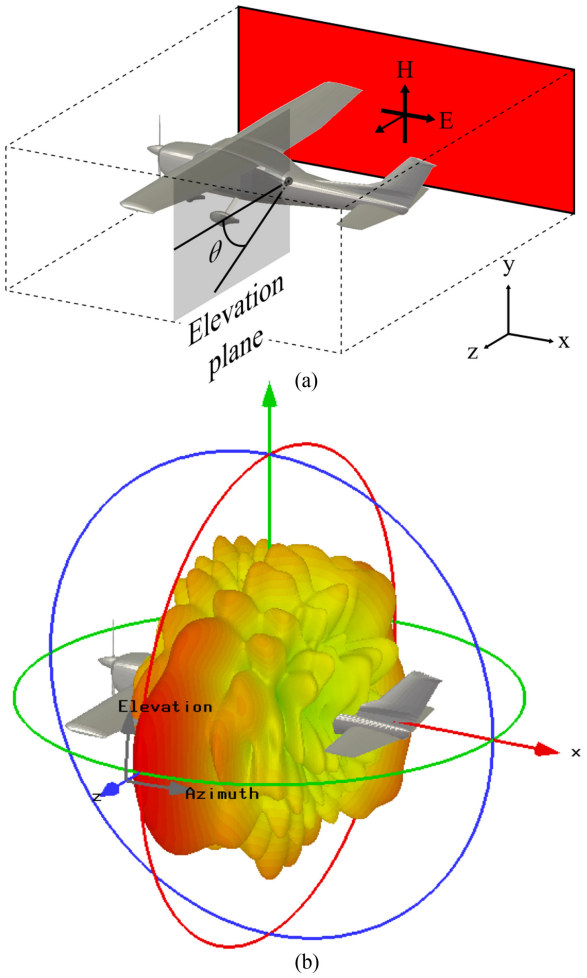

Fig. 4. (a) CST model of Cessna 172. (b) 3-D RCS simulated at 223 MHz shown for 0° illumination angle.

varied from −2° to 5° with 1° intervals. This range of angles matches the geometry of the experimental scenarios.

The simulations have been made at frequencies of 93, 223, and 650 MHz corresponding to FM radio, DAB radio, and DVB-T signals.

An example of the 3-D RCS for 0° angle of illumination is shown in Fig. 4(b). For this study, the elevation plane of the RCS pattern, as defined in Fig. 4(a), is of importance. Fig. 5 shows 2-D RCS pattern at this plane for a target illuminated at broad side (0° angle of illumination), for each frequency of interest. In this figure, an elevation angle of 0° corresponds to the forward-scatter direction.

It should be mentioned here that the RCS patterns do not differ significantly with the change of target illumination angle within the chosen range. The change in both maximum FSCS and ML width can be seen in relation to the frequency. The 15 dB increase of maximum of FSCS magnitude is seen when frequency changes from that of FM radio to DVB-T, while main beam width narrows by approximately a factor of 6.

It should be noted, however, that the forward-scatter regime can be considered to extend to about 40° either side of broadside, even at higher frequencies. At those angles, the FSCS is actually similar at all wavelengths, being the

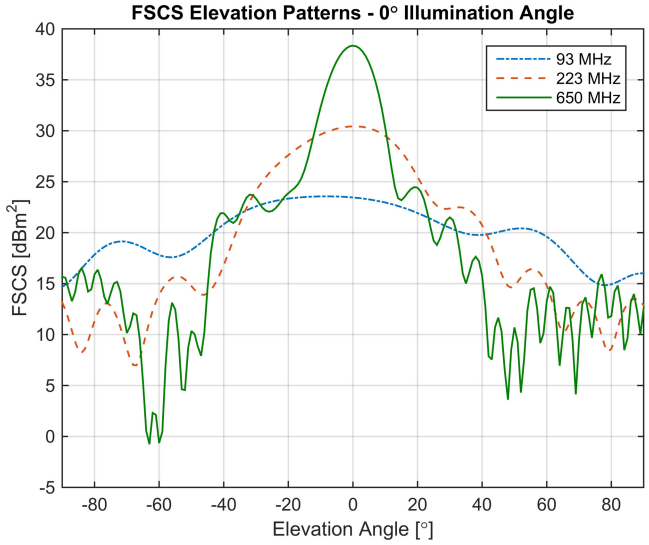

Fig. 5. FSCS elevation patterns for three frequencies with a target illumination angle of 0° elevation is the FS direction.

edge of lower (but wider) pattern at low frequencies and the sidelobes of such higher (but narrower) pattern seen at higher frequencies, at the same power level.

3) Comparison of Analytical Approximation and Modeling: Table I confirms the substantial agreement between the theoretical values obtained by (2) and (4) and the simulations of the FSCS pattern obtained from the accurate CST model.

Given the FSCS values and elevation patterns for different illumination angles, it is now possible to make some estimation of sensitivity and of the maximum altitude at which target can be detected as shown in Section III-B3.

B. Preliminary Power Budget

In a typical scenario, where the transmitted wave is propagating above the surface, there are two signals at the receiving point: direct path or LoS signal and the signal reflected from the ground. The two-ray path model [19] is, therefore, used as a reference model for the estimation of the power level received at a distance d from the transmitter

$$P_{\mathrm{DS}} = 4P_tG_tG_r\left(\frac{\lambda}{4\pi d}\right)^2 \sin^2\left(\frac{2\pi h_t h_r}{\lambda d}\right) \tag{5}$$

where P_t is the transmitted power, G_t and G_r are the transmitter and receiver antenna gains, and h_t and h_r are the heights of the transmitting and receiving antennas above the local ground surface. The surface is assumed to be flat and smooth.

The target scattered signal power level can be calculated with the same model applied to the target signal, as discussed in [19]

$$P_{tgt} = 16P_tG_tG_r\sigma_{fs}\frac{1}{d_t^2d_r^2}\frac{\lambda^2}{(4\pi)^3}\sin^2\left(\frac{2\pi h_t z_{tgt}}{\lambda d_t}\right)\sin^2 \times \left(\frac{2\pi h_r z_{tgt}}{\lambda d_r}\right) \tag{6}$$

TABLE II
Parameters Used in the Power Budget Evaluation

Parameter	Value
f_c (DVB-T)	650 MHz
Δf	8 MHz
P_t	50 dBW
G_t	0 dBi
G_r	8 dBi
h_t	270 m
h_r	1.5 m
z_{tgt}	200 m
σ_{fs}	10 dBm^2
T_{int}	10 s
L_e	10 dB

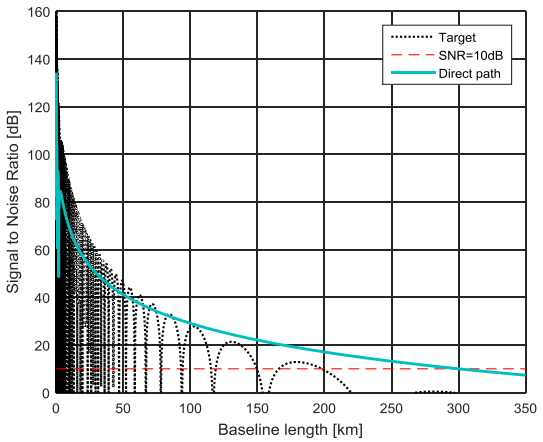

Fig. 6. SNR ratio for the direct signal (dot dashed curve) and for the target signal (solid curve). The dashed curve highlights the lowest received power level to have DVB-T coverage and to guarantee good detection performance.

where z_{tgt} is the altitude of a point like target, d_t and d_r are the distances to the target from the transmitter and the receiver, respectively, and σ_{fs} is the target FSCS.

The power budget analysis considers a system with the parameters shown in Table II.

1) Direct Signal Reception Range: It is appropriate first to calculate the SNR ratio for the direct path signal. This is given by

$$\text{DSNR} = P_{\text{DS}} - N - L_e \tag{7}$$

where N is the receiver noise power in the signal bandwidth, and L_e represents the miscellaneous losses and all the values are in dBm or decibels.

This equation allows us to evaluate the maximum possible separation between transmitter and receiver. If the direct signal (which is usually stronger than signal scattered from the target) cannot be received, then we will not be able to detect the scattered signal. The noise power is given by $N' = kTN_f\Delta f$, where $k = 1.38\ 10^{-23}$ J/K is the Boltzmann constant, $T = 290$ K is the system temperature, $N'_f = 6$ dB is the receiver noise figure, and Δf is the frequency interval of interest, which in our case is the 8-MHz DVB-T signal bandwidth. The results of the DSNR calculation are presented in Fig. 6. The DSNR is shown by the solid curve. The dashed line represents the minimum signal-to-noise ratio, the threshold value which has been set to 10 dB for efficient processing (see Section II-A and [13]). The intersection between these lines indicates that the maximum distance at which the DVB-T coverage is guaranteed is 300 km. It should be remembered, however, that a "flat earth' model is used and, in practice, the earth's curvature will limit the maximum baseline length to around the horizon. For radio frequency signals, the horizon will be at around 70 km since the effective radius of the earth at these frequencies can be taken as 4/3 of its geometrical value.

2) Target Detection Range: The power of the signal scattered from the target will be considered for the worst-case scenario: i.e., a very small target (see Fig. 5—$\sigma_{fs} = 10$ dBm^2), which crosses the baseline at the midpoint, i.e., $d_t = d_r = d_m = L/2$, because it results in the minimum of the scattered power as $P_{tgt} \propto 1/(d_r^2 d_t^2)$. In this case, SNR $= P_{tgt} - N_0 - L$, where $N_0^{'}$ is the noise power after matched filtering (which by definition gives the best potential SNR), so the bandwidth is the inverse of the visibility time (T_{int}) (i.e., $\Delta f = 0.1$ Hz) and all the values are in dBm or decibels. The result using values in Table II is shown in the solid curve in Fig. 6. It is apparent that an SNR of 10 dB is attainable for baselines up to 150–200 km in this flat earth scenario. Considering fading margin of 10 dB, this will be reduced to 100–150 km still suitable for the wide-area surveillance.

The power budget analysis, therefore, shows that systems using broadcasting transmitters can detect even small targets at long range. This analysis will also be used in Section V-A for the power budget estimation in the real-experimental scenario. Now, we can concentrate on the constraints of the experimental scenarios for small target detection.

Detection at long range is more likely to be susceptible to interference from signals from other transmitters on the same frequencies. However, the forward-scatter receiver can avoid corruption of the data by making use of the usual coordination systems employed by the communications systems to protect their own receivers from such effects. Such techniques include the design of frequency reuse patterns and the use of coordinated waveforms in "signal channel" networks can be exploited by the forward-scatter receiver to avoid corruption of the data. It is also unlikely that targets will be seen simultaneously in forward-scatter configurations between multiple transmitters and a given receiver and the success of the trials supports this view.

3) Maximum Target Altitude: We may assume that detection occurs if the FSML is directed toward the receiver down to −3 or −10 dB off-axis levels. A single baseline length of 25 km is considered here. The maximum target altitude z_{tgt} is estimated for different target crossing distances d_R from the receiver starting from the middle (see Fig. 3). The transmitter height of 270.5 m corresponds to that of the broadcast transmitter in Sutton Coldfield, U.K. (see Section IV) and the maximum altitudes are capped to 1.4 km to limit the range of simulation required. For the lowest frequency (FM radio), the −10-dB result is not shown as the target ML is always visible to the receiver for the altitudes considered here. This is also true for the −3-dB ML, except for when is very close to the receiver,

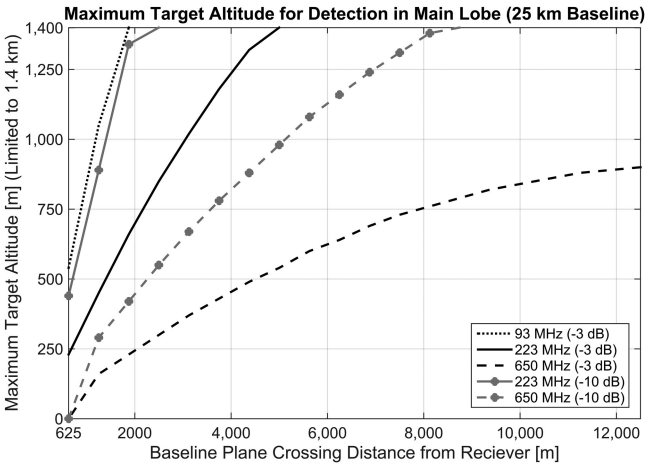

Fig. 7. Maximum target altitude for detection within −3 dB (lines without markers) and −10 dB (lines with markers) FSCS ML as a function of the distance from the receiver and frequency of illumination.

and the same is true for the DAB frequency when considering the −10-dB lobe width. However, at this frequency, detection within the −3-dB width at the maximum altitude of 1400 m is only attainable at crossing distances of more than 5000 m from the receiver.

The effect of the narrowing of the main FSCS lobe at DVB-T frequencies (650 MHz) for this baseline length dramatically reduces the maximum target detection altitude: specifically, when considering the −3-dB width, the maximum altitude reaches about 900 m for the midpoint baseline crossing.

The above analysis assumes that detection is always possible given the FSCS values obtained. For increased baseline lengths, which may involve detection at longer ranges, higher frequency passive signals would be preferable. In fact, due to the increase in FSCS, the limitation of narrower ML width is compensated by the reduction in angles due to the longer baseline length itself.

The analysis has not considered how the elevation coverage of the transmitter affects the coverage. Hagan *et al.* [20] suggest that the designed elevation coverage of DVB-T transmitters may limit the effectiveness of such signals for detection of targets at higher altitudes, but Young *et al.* [21] show experimental results that are better than [20] would suggest, a phenomenon which is perhaps attributable to the actual installed elevation patterns of the transmitters being rather less well controlled than would be expected from the laboratory.

IV. MEASUREMENTS. AIRLINER TRIALS

A. Radar System Setup

A single baseline passive FSR system was set up to test the performance of the algorithm described in Section II. The Sutton Coldfield, U.K., broadcast transmitters [22] were used as IoOs. Its antennas are 440 m above sea level (a.s.l.), which corresponds to a 270-m tower and 170-m terrain height. The station broadcasts analogue and digital signals for both radio and television services with the parameters shown in Table III. This transmitter was chosen because of its wide range of transmitter frequencies and their high power levels.

TABLE III
Sutton Coldfield Transmitted Signals Used in Our Experiments With Their Frequencies and Powers

Signal	Frequencies [MHz]	Signal Bandwidth [MHz]	Transmitted Power[kW]
FM	88.3	0.150	250
	90.5		250
	92.7		250
	95.6		11
	96.4		10
	97.9		250
DAB	222.06	1.536	8.7
	225.65		10
DVB-T	650	8	200
	674		200

TABLE IV
Parameters of the UoB Experimental Receiver

Tunable frequency range	50 MHz to 2.2 GHz
Antennas	DVB-T—Yagi, gain—8 dBi DAB—three-element DAB commercial antenna gain—6.2 dBi FM—Yagi FM antenna Gain—5 dBi
Number of channels	2
USRP channel bandwidth	10 MHz
Azimuth coverage	DVB-T—20° DAB—60° FM—110°
Elevation coverage	DVB-T—20° DAB—60° FM—70°
Consumed power	90 VA

The experimental receiver of the University of Birmingham (UoB) was designed around a National Instruments USRP-2950R [23] software defined radio which contained two full-duplex transceivers, controlled by a host laptop running LabView.

Parameters of the receiver are summarized in Table IV. During the initial experiments, only DVB-T and FM signals were exploited, while for those described in Section V-B, DAB signals were also used.

In each recording, a pair of signals (i.e., either DVB-T and FM, or DVB-T and DVB-T) was acquired simultaneously by the two USRP receiving channels. One of the constraints imposed by the USRP is that both acquired channels must be sampled at the same rate. This is obviously set by the signal with the larger bandwidth. In our case, this corresponds to the 8-MHz bandwidth of DVB-T. In order to make acquisitions in the most efficient way, we decided to record signals in both USRP channels with over 10-MHz bandwidth, which is slightly larger than the DVB-T channel width. So the final sampling rate was 20 MHz for each RF channel. For both USRP channels, the center frequency was chosen to allow recording of as many available broadcast channels as possible. Thus, all six FM frequencies, shown in Table III, were recorded simultaneously.

TABLE V
Fresnel Parameter Estimation

Signal	Fresnel parameter S [m]	Target Electrical Dimension	FS ML [Deg]
FM [90 MHz]	86.7	10.2	$(\theta_h, \theta_v) = (5.6; 16.3)$
DVB-T [650 MHz]	626.2	73.7	$(\theta_h, \theta_v) = (0.8; 2.3)$

In the two scenarios of the experiments presented in this paper, the receivers were placed so as to provide far-field operation at all the frequencies used. Moreover, we are interested in operating in the optical scattering regime to exploit the increased FSCS (4) in order to deliver the required detectable power of the scattered signal. The above conditions are satisfied if

1) the target size is significantly smaller than its distances from both the Tx and the Rx. This means that both distances must be greater than the Fresnel length $S = D^2/(4\lambda)$ [15];
2) the target dimensions are much bigger than the signal wavelength, i.e., the target is electrical large: $D/\lambda >> 1$ [2].

Table V shows the values of the target electrical dimension corresponding to each frequency band, and, hence, of the lobe width, which match the extreme values of the Fresnel parameter. The latter was defined as a conservative estimate using $D \equiv 34$ m, this being the greatest dimension (between wingspan and body length) of the largest measured aircraft, as presented in the Section IV-B. The largest S is defined by DVB-T signal frequencies and requires that the receiver to be at a minimum distance of 626.2 m from the crossing point.

On the other hand, the optical scattering condition will be less easily satisfied at FM signal frequencies for smaller aircrafts, discussed in the Sections V-A and V-B, as is also apparent from the FSCS peak gain shown in Fig. 5. This case is closer to Mie scattering, but does not significantly affect the results of detection.

Therefore, whereas for DVB-T, we have guaranteed the strong FS CS increase within its ML [2] for FM we have a border line situation.

The initial experiments, presented in Section IV-B, were conducted near Birmingham International Airport (BHX), U.K., where we aimed to record signatures of planes taking off and landing. The crossing point was, therefore, at 6 km from site Rx1 and 15 km from site Rx2, as shown in Fig. 8(a). The distance between BHX and the Sutton Coldfield transmitter is about 20 km, making the baselines 26 and 35 km to Rx1 and Rx2, respectively. In both experiments, the constraint for far-field operation was satisfied for all the frequencies used.

To obtain ground truth, all recorded passenger airplanes have been tracked using Flightradar24 [24], which provides information on their altitude (a.s.l.), location, and speed with good accuracy. Due to the geometry between the transmitter and the airport flight path [cyan line in Fig. 8(a)], the

(a)

(b)

Fig. 8. Trials topology shown in Google Earth [25]. (a) Receiver Rx1 site at 6 km and (b) distance from crossing point, with FM and DVB-T antennas.

trajectories of each aircraft were similar, with a small crossing angle of about 15°.

B. Experimental Results

The recorded signals have been processed using the approach described in Section II. For the DVB-T signals, the passband of the BPF was set at the signal bandwidth (8 MHz), while a cutoff of LPF was 100 Hz. For the FM signals, an additional preprocessing step was undertaken which comprised separation of the different FM channels and decimation to a lower sampling rate in accordance with the Nyquist criterion for FM broadcasting channel bandwidth of 150 kHz. Then, the upper cutoff frequency of the BPF (see Fig. 1) was set to 150 kHz and for the LPF (after the hard limiter), it was set to 100 Hz. The decimation block decimated signals to a fixed sampling rate of 200 Hz.

The experimental results presented in this section are Doppler signatures and their spectrograms, obtained at the output of the processing chain shown in Fig. 1 (point E), which allows visualization of the amplitude modulation due to the target crossing the baseline. The time-domain signatures are shown together with the short-time Fourier transform of the signatures. To ease the comparison of the spectrograms, they have been normalized so that the maximum levels of the FM and DVB-T signals are the same color.

The first experiment, with the receiver at position Rx1, providing 26-km baseline [see Fig. 8(a)], was car-

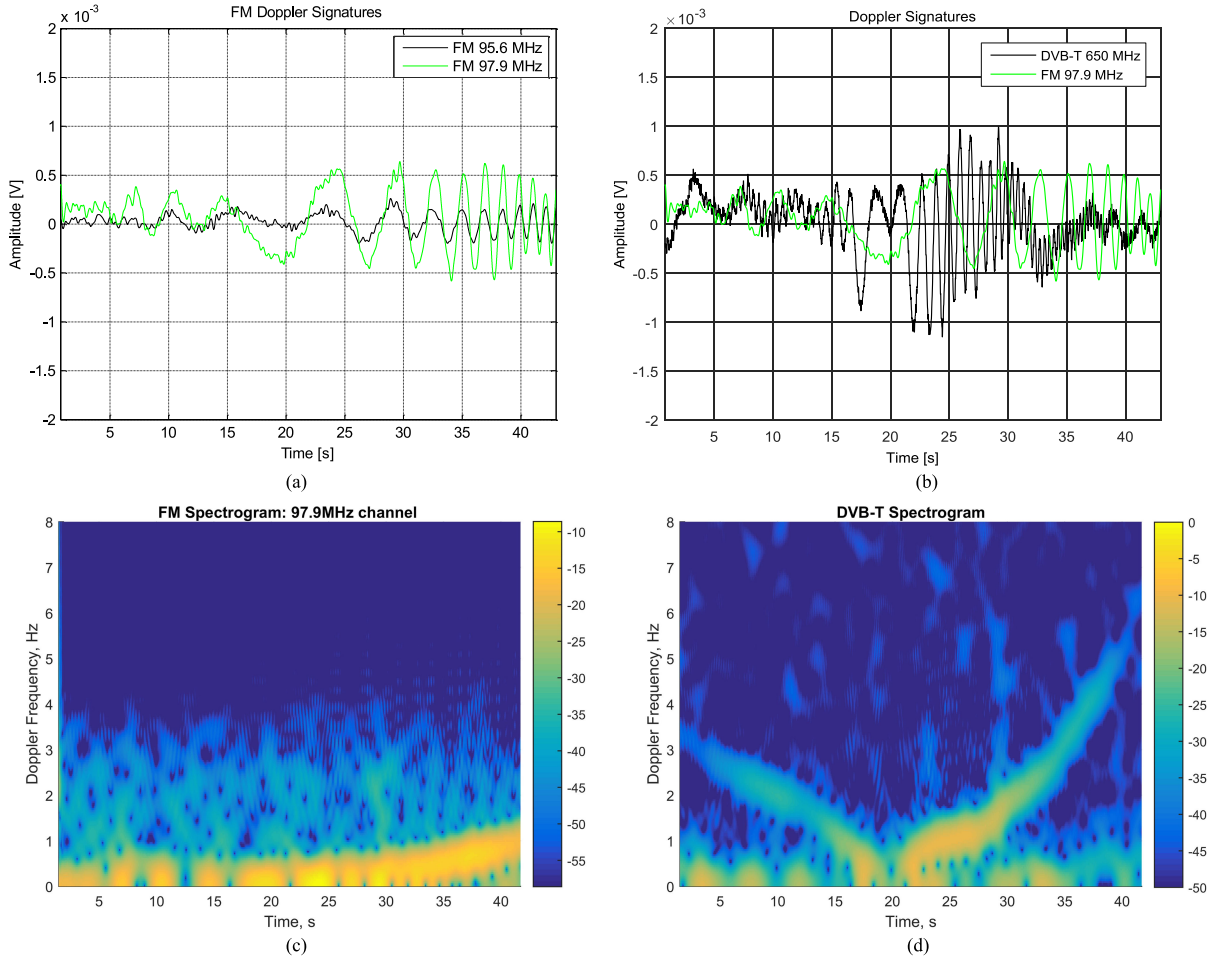

Fig. 9. FM and DVB-T Doppler signatures (a) and (b) and spectrograms (c) and (d) of the taking off Airbus A320. The baseline is 25 km.

ried out to record FM and DVB-T signals, as explained in Section IV-A. Fig. 9 shows the Doppler signature of an ascending plane after take off from BHX. The aircraft was an Airbus A320 with dimensions of 33.8 m length, 11.7 m height, and 34.1 m wingspan. It was at 180 m altitude when crossing the baseline. The speeds given by Flightradar24 for this takeoff phase are between 240 and 285 km/h.

Doppler signatures were extracted from all six FM channels from 88.3 to 97.9 MHz and all of them are slightly scaled version of each other. To avoid dense plotting of very similar signals, only two of them are shown in Fig. 9(a). The gradual increase of the oscillation rate of the signatures due to acceleration during take-off stage is clearly visible. It is worth nothing that the signature in the 95.6-MHz channel is as clear as the one from the 97.9-MHz channel, although the former has 14 dB less transmitter power (see Table III). This demonstrates good robustness to a variety of situations involving different SNR's.

For comparison, the signatures extracted from FM (97.9 MHz) and DVB-T (650 MHz) signals are shown in Fig. 9(b). Although there is a clear correspondence between the trends of the Doppler frequency in the two signals, with the crossing point being visible at 20 s, the Doppler frequencies of the FM signals are a factor of 6,5 lower than those of the DVB-T signals, exactly as would be expected from the ratio between their carrier frequencies. Indeed corresponding spectrograms, shown in Fig. 9(c) and (d), show that the maximum Doppler frequency of the signature with the FM signal is about six times smaller than that of DVB-T signal.

The smaller Doppler at the start of the record indicates the fact that the target speed is low at the start of the plane's ascent. Also in Fig. 9(c) and (d), the highest signal intensity corresponds to the target FSCS ML (15–23 s for FM and 17–22 s for DVB-T) and decreases in the side lobes.

It can be seen from the color scales of the two spectrograms that the maximum of the DVB-T signals is 10 dB higher than that for the FM spectrogram. Since the effective radiated power and receiver aperture are greater for the FM signal and the receiver gains are the same at both frequencies, this difference shows that the directionality seen from the target is much bigger at the higher frequency, as predicted by (4).

The second experiment was made with the receiver positioned at Rx2, resulting in a baseline of 35 km, as shown in Fig. 8(a). On this occasion, the aircraft were crossing the baseline during descent for the landing, because the wind was blowing from a different direction. Two different combinations of broadcasting signals were recorded: two DVB-T channels [see Fig. 8(c)] and one DVB-T with one FM channel.

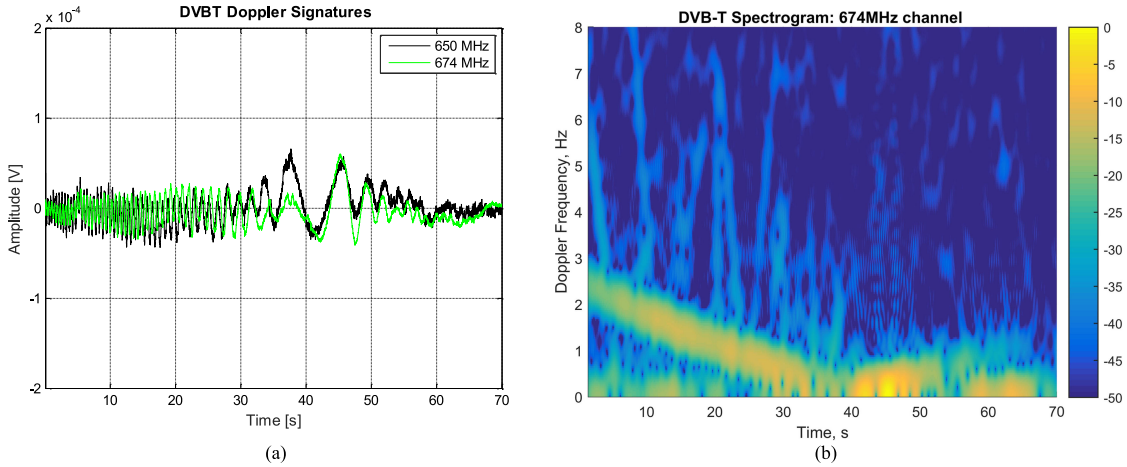

Fig. 10. DVB-T Doppler signatures (a) and spectrograms (b) of a landing Bombardier Dash8 Q-400. The baseline is 35 km.

TABLE VI
Fresnel Parameter, Electrical Target Dimensions, and FS ML of the Cessna Target at FM, DAB, and DVB-T Frequencies

Signal	Fresnel parameter S [m]	Target Electrical Dimension	FS ML [deg]
FM [90 MHz]	9.1	3.3	$(\theta_h, \theta_v) = (17.4, 83.0)$
DAB [225 MHz]	22.7	8.3	$(\theta_h, \theta_v) = (6.9, 33.2)$
DVB-T [650 MHz]	65.5	23.8	$(\theta_h, \theta_v) = (2.4, 11.5)$

The increased distance from the target path to the receiver slows everything down. For a given carrier frequency, the Doppler will vary more slowly within the observed narrow FS area, but, since the crossing angle is the same, the angular interval for which the target is observed (and therefore the observation time) will increase. The lower rate of change of the Doppler frequency is clearly visible for the DVB-T signal and, obviously, it affects the appearance of Doppler signature of FM signal so that a very long record length is needed to reach a Doppler frequency above 1 Hz. Below this Doppler shift, the spectrum is more likely to be contaminated by clutter [26].

Two simultaneously recorded signatures at two DVB-T channels centered at 650 and 674 MHz, respectively, are shown in Fig. 10 for a Bombardier Dash8 Q-400 aircraft, with dimensions of 32.8 m length, 8.3 m height, and 28.4 m wingspan. According to Flightradar24 at the crossing instant, it was at 236 m altitude with a speed of 263 km/h. The two signatures are very similar except for a phase difference due to the use of two physically separate antennas. The spectrogram in Fig. 10(b) clearly demonstrates the deceleration of the descending aircraft. From the comparison of Fig. 9(a) and (b) and Fig. 10(a), it is also seen that the combination of a crossing point closer to the middle point and the decreased FSCS value in the direction of Rx, due to the higher flight height, lead to reduction of received scattered power.

V. LIGHT AND ULTRALIGHT AIRCRAFTS TRIALS

A. UoB Scenario and Results

In order to investigate the system performance for the detection of small light low flying aircraft, another set of experiments has been conducted for which a Cessna 172 light aircraft shown in Fig. 11(b) was used, as a controlled target. Its dimensions are 7.3 m length, 2.3 m height, and 11 m wingspan. Fig. 6.

In this experiment, the receiver was set in the open-field near Sibson, close to Leicester, U.K. As in Section IV , Fresnel parameter, target electrical dimension, and FS main lobe of the target at each frequency band have been calculated, and a summary is shown in Table VI. The site is at 81.5 m height a.s.l., at 25 km distance from the Sutton Coldfield transmitter. There was a clear LoS between Tx and Rx. In addition to the receivers used for the airliner measurements, in this case, a three-element DAB commercial antenna was available with a -3-dB beamwidth of 60° in both horizontal and vertical planes and having 6.2-dBi gain. The site and scenario were chosen to satisfy two requirements.

1) The target can fly at a relatively low height (for rural area a limit of 450 m).
2) To be able to avoid the air traffic control constraints in the region of BHX.

The trials were conducted with the target following the "racetrack" shown in Fig. 11(a) which was selected, in consultation with the pilot, to cross the baseline almost perpendicularly at a point approximately one third of the way along the baseline, while maintaining a safe flight path.

The aircraft altitude increased by nominally 100 m on each circuit, in order to determine the system's ability to detect targets flying at different altitudes.

The results presented and discussed in this section correspond to three representative altitudes: the lowest of 450 m a.s.l, the highest of nearly 1 km, and an intermediate value of about 800 m, as shown in Table VII. The start times of the recordings were synchronized with a GPS tracking device onboard the aircraft. The GPS ground truth data are shown in Table VII.

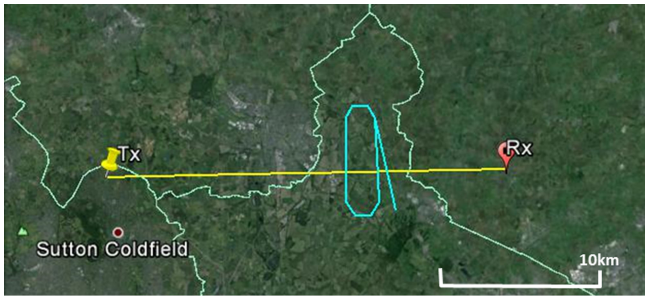

(a)

(b)

(c)

(d)

Fig. 11. (a) Trials topology on Google Earth; (b) Cessna 172 ultralight aircraft; (c) receiver DVB-T and DAB antennas; and (d) USRP and the laptop.

TABLE VII
GPS Ground Truth of Three Acquisitions With Cessna

Data	Crossing distance from Rx[km]	Crossing Angle [deg]	Crossing Height a.s.l. and above baseline)[m]	Recorded Signals
D1	9.1	86	483 (354)	DVB-T + DAB
D2	9.0	87	788 (659)	DVB-T + FM
D3	7.9	85	947 (833)	DVB-T + FM

The bandwidth of the receiver used for DAB signals comprises two DAB channels centered at 222.0 and 225.65 MHz (see Table VII), so as with the FM signal, an initial processing step was incorporated to separate them. Then, after the BPF with a cutoff frequency of 750 kHz, decimation was applied to reduce the sampling rate and the LPF cutoff frequency was again set to 100 Hz.

The results of the first acquisition D1 (see Table VII) at 650 MHz shows that even though the target is much smaller than the airliner seen in the previous section, the Doppler signature in Fig. 12(a) is well defined although the power

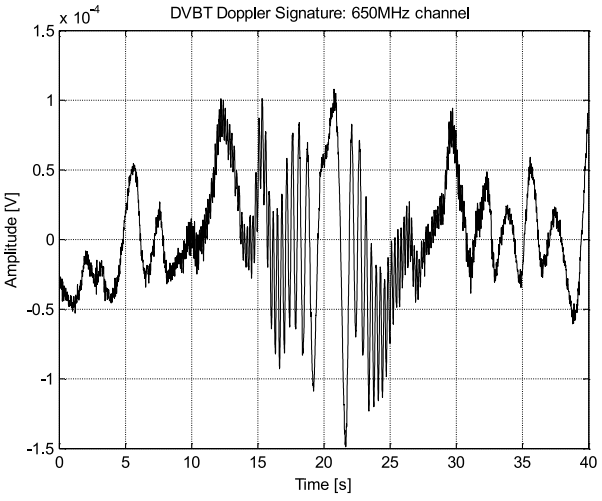

(a)

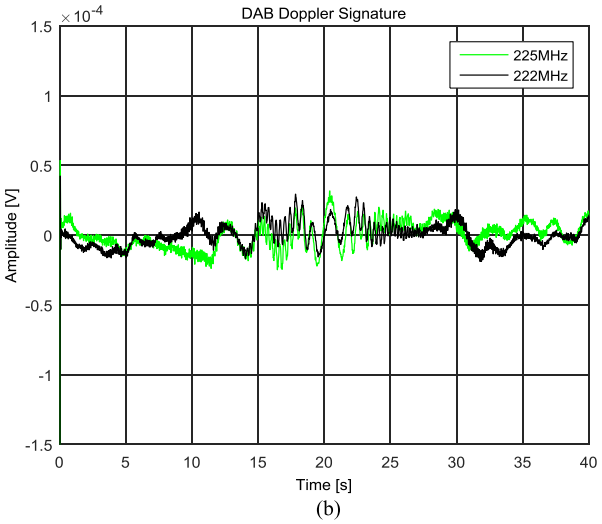

(b)

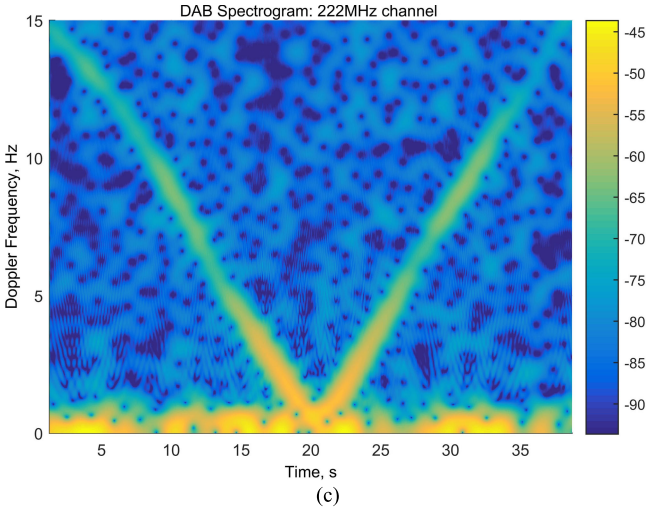

(c)

Fig. 12. DVB-T and DAB acquisition of Cessna at 354 m above the baseline (D1).

of the scattered signal is smaller compared with that of the airliner, as shown in Fig. 9(a). Moreover, the different flight stages when the target is approaching, crossing, and departing from the baseline can be easily distinguished not only in the DVB-T signals but also in theDAB signatures

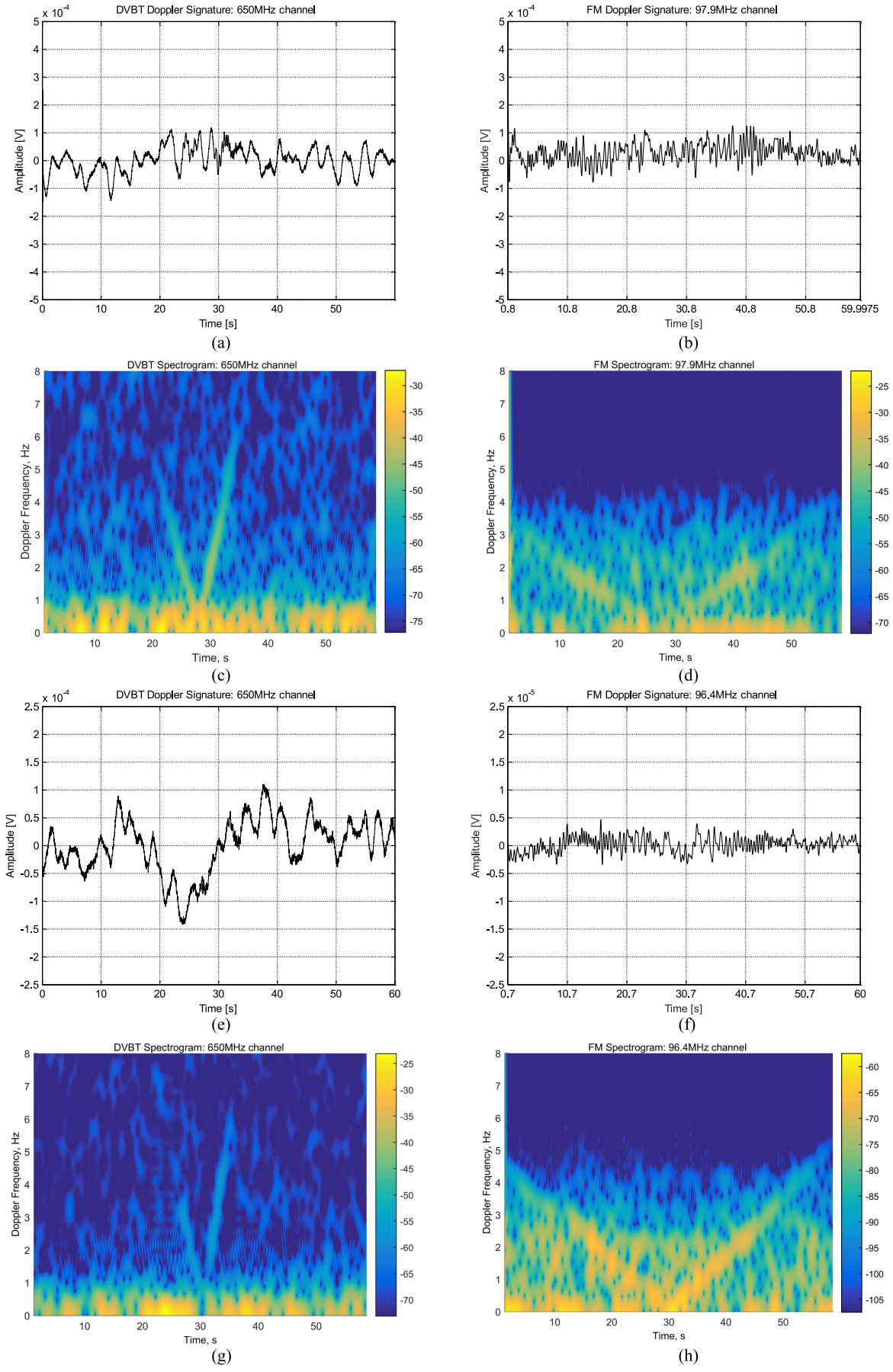

Fig. 13. DVB-T and FM Doppler signatures and spectrograms of Cessna at 659 m (a)–(d) and 833 m (e)–(h) above the baseline (D2 and D3).

signals in Fig. 12(b) despite the fact that the transmitted power is 14 dB lower.

The two branches of the spectrogram in Fig. 12(c) are symmetrical, due to the orthogonal crossing and constant speed. Moreover, the wider FS ML of the smaller target leads to an increase of the time interval in which the Doppler chirp with a frequency sweep up to 15 Hz is clearly visible.

The effect of the vertical distance Δh_c between the flight trajectory and the baseline (see Table VII) is seen from comparison of the spectrograms of the D1, D2, and D3 data. The latter correspond to the FSML, no longer impinging on the receiver, resulting in a reduced received power. The wider target FS ML seen at FM frequencies guarantees that the receiver is illuminated by the FSCS ML in a wider range of plane altitude with respect to DVB-T. However, as apparent from Fig. 5, the target FSCS at 650 MHz has higher gain than for FM, not only in the ML but also in the first two sidelobes. Hence, in the D2 and D3 acquisitions, where the target is in a lower gain region at the DVB-T frequency, but still inside the -10 dB ML (see Fig. 7), the intensity of the FM and DVB-T spectrograms (see Fig. 13(c) and (d)—D2, and Fig. 13(g) and (h)—D3) is comparable, as expected from Fig. 5.

As expected, increasing the flight altitude results in smaller signal powers, and, therefore, in the more noisy picture seen in Fig. 13(e) and (f), but the typical V-shape Doppler chirp which indicates the presence of a target can still clearly be seen in the spectrograms.

Other analysis has shown that for the conditions used for this experiment, the estimated SNR is approximately 45 dB, while the model predicts 47 dB using the effective LPF bandwidth to calculate the noise power.

The two-ray path model presented in Section III-B has, therefore, delivered SNR values which are in good agreement with the measurement results.

B. FHR Scenario and Results

Trials with the Fraunhofer FHR experimental passive radar system (PARASOL) took place in Eckernförde [see Fig. 14(a)], north of Germany, in the Bundeswehr Technical Center for Ships and Naval Weapons. The system was mounted on the workboat AM8 [see Fig. 14(c)] which was moving inside the Eckernförde bay.

The PARASOL system operates with two parallel receiving channels, each consisting of an RF module and an ADC/FPGA module. Both channels feed into a high-performance PC module. The log-periodic antennas, the hardware, and the processing are optimized for exploiting DVB-T as the IoO. The receiver local oscillators are locked to GPS. Table VIII summarizes the main characteristics of the PARASOL system.

For this study, the system used the transmitter located in Kiel [see Fig. 14(a)]. The main characteristics of the transmitter are summarized in Table IX, while Fig. 14(a) shows a sketch of the acquisition geometry.

An ultralight Delphin aircraft [see Fig. 14(b)] was used as a cooperative target during the experiment, flying around the Eckernförde bay. Its dimensions are 6.5 m length, 2.2 m height, and 9.4 m wingspan. At certain points in its trajectory, the mutual position of transmitter, target, and receiver leads to a forward-scatter geometry with a bistatic angle close to 180°. Such geometry is unfavourable for conventional passive bistatic radar processing, yet target detection is still possible by exploiting the P-FSR target signature processing proposed in this paper.

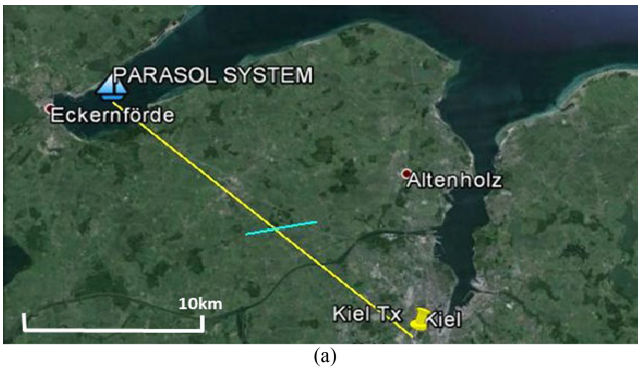

(a)

(b)

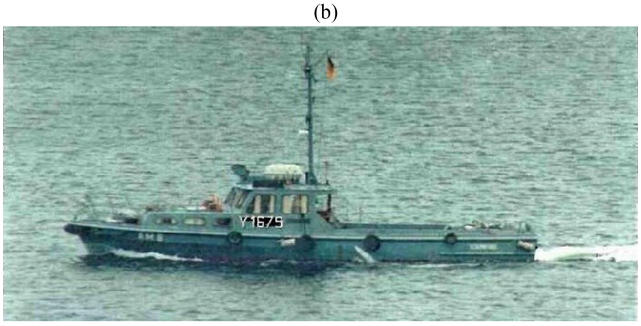

(c)

Fig. 14. (a) Scenario of the FHR trial in Eckernförde. The blue marker indicates the position of the PARASOL system; the cyan line indicates the trajectory of the ultralight aircraft Delphin, the yellow line is the baseline, and the yellow marker indicates the position of the transmitter. (b) Ultralight aircraft Delphin. (c) Workboat AM8, where the PARASOL system was mounted.

TABLE VIII
Parameters of the PARASOL System

PARASOL SYSTEM	
Band	470–780 MHz
Number of antennas	2
Antenna	one vertically and one horizontally polarized log-periodic antennas
Number of channels	2
Bandwidth channel	7.61 MHz
Azimuth coverage	60°
Elevation coverage	60°
Real-time processing	Yes
Consumed power	500 VA

TABLE IX
Characteristics of the Kiel Transmitter

Signal	DVB-T
Frequency	666 MHz
Modulation	16 QAM
Site Elevation	38 m
Antenna Height	219 m
ERP (kW)	43
Polarization	H

The motion of the receiver was tracked by a spatial dual inertial measurement unit (IMU) [27]. The IMU has been placed high on the antenna mast, close to the antenna elements so that they may experience motion components very similar to those acting on the measurement antennas.

Applying the processing described in Section II to the data acquired, the FSR Doppler signatures were extracted and two of them corresponding to orthogonal polarizations of the receive antennas are shown with their spectrograms in Fig. 15.

The comparison of the powers of the two Doppler signatures plotted together in Fig. 15(a) and in the spectrograms in Fig. 15(b) confirms that the target scattered signals in the FS direction maintain the same polarization as the transmitted signals [15]. The spectrograms give further insight: in the spectrogram of the horizontally polarized channel of Fig. 15(b), there is a bright spot which occurs at the target baseline crossing time (around 27 s) and indeed corresponds to the peak of the FSCS, which conversely is far less pronounced in the vertical polarization spectrogram of Fig. 15(c).

It is noticeable that after the forward-scatter signal disappears from the horizontally polarized channel, the vertically polarized channel continues to show what appears to be the Doppler signature of the target, but now moving with constant speed. One possible explanation may be that the returns due to the progression into a more bistatic configuration—the "wing" on the spectrogram—corresponding to the target departing from the baseline have, as expected from theory, approximately the same intensity in both polarizations due to the depolarization of the transmitted signal after bistatic scattering from the target.

VI. SPEED ESTIMATION

As one of the main drawbacks of FSR is the absence of range resolution, the trajectory parameters of the target cannot be retrieved through the methods used in monostatic and bistatic radar. As discussed above, "SAR-like" matched filtering to the possible Doppler trajectories [4] is a quasi-optimal approach, which is used to extract these parameters in FSR, where the received target signature is correlated with a bank of waveforms generated for a range of expected values of speed, crossing point, and crossing angle.

It was shown in [4] that this procedure is significantly less sensitive to the amplitude of the signature, defined by the FSCS, than it is to the Doppler shifts on the signal. Another way to do this estimation is to use spectrograms directly [28].

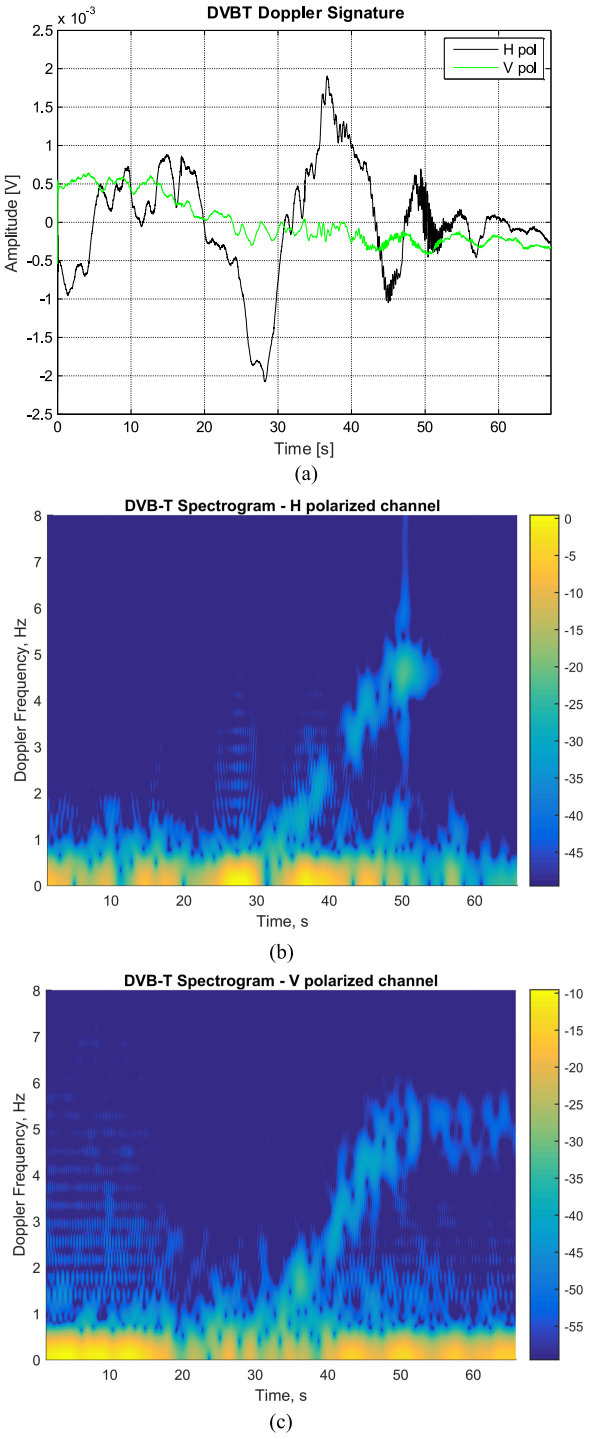

Fig. 15. DVB-T Doppler signatures (a) and spectrograms of Delphin in the horizontally (b) and vertically (c) polarized channels.

Such processing was applied in two cases discussed in the paper: 1) Airliner detection by two DVB-T signals presented in Section IV and 2) Cessna detection by DAB and DVB-T, as shown in Section V-B. The estimated speeds and those provided by ground truth are given in Table X together with the parameters of the signals of opportunity. Very good agreement with ground truth was achieved for both illuminators, for both target types, and for both types of ground truth (IFF from Flightradar24 and GPS).

TABLE X
Comparison of Speed Estimation With Suboptimal Processing and Ground Truth

Data	Signals	Frequency MHz	Estimated speed km/h	Ground Truth km/h
4	DVB-T	650	248.4	263 by Flightradar24
	DVB-T	674	216.0	
D2	DAB	222	176.4	167 by GPS
		225	176	
	DVB-T	650	188.1	

VII. CONCLUSION AND FUTURE PLANS

In this paper, the effectiveness of the passive FSR detection has been demonstrated by exploiting broadcast transmitters of opportunity. A simple approach has been proposed to extract the forward-scatter Doppler signature of target from the signals of terrestrial broadcasting systems, such as DVB-T, DAB, and FM. The independence of the FSR signature from the modulation of the transmit signal has been demonstrated both analytically and experimentally. This shows the universality and wide applicability of the FSR approach for target detection in passive coherent location systems.

Experimentation trials have been conducted to study the system performance for a range of different scenarios and airborne targets in multifrequency/multimode setting. The feasibility of a passive FSR for airborne target detection has been demonstrated for the first time using FM, DAB, and DVB-T waveforms. It has been shown that simultaneous multifrequency/multiband operation increases robustness of detection. While higher frequencies lead to higher accuracy of kinematic parameters estimation, the lower frequency signals define a larger FSR operational region. Moreover, it has been experimentally demonstrated that the transmitted powers of available IoOs provide the required sensitivity for detection of airborne targets ranging from an ultralight aircraft to airliners at altitudes up to 1000 m.

In addition, the speed of the detected targets has been estimated using quasi-optimal processing and good correspondence to ground truth data has been demonstrated. This allows the conclusion that P-FSR is a practical solution not only for detection of the target, but also for the estimation of its kinematic parameters. As the next step, we plan to investigate the feasibility of extracting kinematic parameters from the spectrograms, which should be more robust to presence of clutter and noise than was the time-domain signature. Furthermore, aircraft target profile reconstruction by its Doppler signature [29] will be investigated.

APPENDIX

A. Independence of Doppler Signature on Communication Signal Modulation

The aim of this appendix is to show analytically that the results of the processing used to extract the Doppler signature from the FSR signal is independent of the modulation on the illuminating signal as was initially stated in [2].

As noted above, the IoO's considered for the system experimental validation were DVB-T, DAB, and FM signals.

1) *Digital Modulated Signals: DVB-T and DAB:* DVB-T and DAB are digital broadcasting standards defined by the European Telecommunications Standards Institute [9], [10], respectively, for video and audio signals. These standards use orthogonal frequency-division-multiplexing (OFDM) transmission to transfer both signaling information and data. All the data carriers in one OFDM frame are modulated using phase-shift keying, quadrature amplitude modulation (16 QAM), or 64 QAM constellations. Since both the audio and the video standards share the same principal signal features (the main difference is the signal bandwidth), the analytical derivation is presented only for DVB-T. Obviously, the same approach can be applied to DAB so the conclusions of this section are straightforwardly applicable to DAB.

From [9], the transmitted DVB-T signal can be described by the following expression:

$$s_{\mathrm{DVB-T}}(t) = \Re e\left\{\left(\sum_{m=0}^{\infty}\sum_{l=0}^{67}\sum_{k=K_{\min}}^{K_{\max}} A_{m,l,k}e^{j2\pi f_k t_{m,l}}\right)e^{j\omega_c t}\right\} \tag{8}$$

where

m	transmission frame number;
l	OFDM symbol number;
k	subcarrier number $K_{\min} \le k \le K_{\max}$;
$A_{m,l,k}$	constellation complex value for carrier k of data symbol $l+1$ in frame number m;
$f_k = k'/T_u$	kth subcarrier frequency and $k' = k - (K_{\max} - K_{\min})/2$, where T_u is the inverse of the carrier spacing;
$\omega_c = 2\pi f_c$	frequency Doppler shift and f_c is the carrier frequency;
$t_{m,l}$	time interval in which the symbol of frame m is defined.

Since the first two sums in (8) change the frame and the symbols, respectively, for the sake of providing a clearer explanation, we can limit the analytical derivation to a time interval with duration of a single symbol (i.e., in the following, it is assumed that $t = t_{m,l}$). As in [15], the signal at the receiver input $s_{\mathrm{Rx-RF}}(t)$ in (9) has been modeled as the sum of the leakage signal $S_{\mathrm{DP}}(t)$ and the target signal $S_T(t)$ with amplitude A_T and term $\exp(j\omega_d t)$ related to the Doppler shift of the scattered signal, where $\omega_d = 2\pi f_d$ is the angular Doppler frequency

$$\begin{aligned} s_{\mathrm{RX-RF}}(t) &= s_{\mathrm{DP}}(t) + s_T(t) \\ &= \Re e\left\{\sum_{k=K_{\min}}^{K_{\max}} A_k e^{j2\pi f_k t}e^{j\omega_c t}\left(1 + A_T e^{j\omega_d t}\right)\right\}. \end{aligned} \tag{9}$$

In the receiver, this signal is down converted to low IF, and filtered to remove the noise outside the band of interest. Hence, the signal after BPF might be considered as a linear combination of sinusoids with frequencies equal either to one of the subcarriers used in transmission or to the latter

shifted by the Doppler frequency

$$A_{\mathrm{DVB-T}}(t) = \left[\sum_{k=K_{\min}}^{K_{\max}} A_k \cos(\omega_k t)\right] + A_T\left[\sum_{k=K_{\min}}^{K_{\max}} A_k \cos(\omega_k t + \omega_d t)\right]. \quad (10)$$

At this point, the proposed algorithm produces the reference signal by applying the hard limiter to the signal $A_{\mathrm{DVB-T}}$, hence at Point B, the resulting signal is $B_{\mathrm{DVB-T}}(t) = \mathrm{sign}(A_{\mathrm{DVB-T}}(t))$. As mentioned before, the signal at Point C is mathematically equivalent to the absolute value of $A_{\mathrm{DVB-T}}(t)$, when the multiplied signals are real, as in our case. The analytical derivation of the multiplication between $A_{\mathrm{DVB-T}}(t)$ and $B_{\mathrm{DVB-T}}(t)$ is given by the equivalence relation $|(\cdot)| \equiv \sqrt{(\cdot)^2}$, thus the signal at Point C is the square root of $C'_{\mathrm{DVB-}T}(t)$ in

$$\begin{aligned} C'_{\mathrm{DVB-T}}(t) = A^2_{\mathrm{DVB-T}}(t) &= \left[\sum_{k=K_{\min}}^{K_{\max}} A_k \cos(\omega_k t)\right]^2 \\ &+ A_T^2\left[\sum_{k=K_{\min}}^{K_{\max}} A_k \cos(\omega_k t + \omega_d t)\right]^2 \\ &+ 2A_T \sum_{k=K_{\min}}^{K_{\max}} A_k \cos(\omega_k t) \sum_{j=K_{\min}}^{K_{\max}} \\ &\times A_j \cos(\omega_j t + \omega_d t). \end{aligned} \quad (11)$$

Each of the three terms in (11) is separately expanded and analyzed as

$$\left[\sum_{k=K_{\min}}^{K_{\max}} A_k \cos(\omega_k t)\right]^2 = \sum_{k=K_{\min}}^{K_{\max}} \sum_{\substack{j \\ j\neq k}} A_k^2 \cos^2(\omega_k t) + 2A_k A_j \cos(\omega_k t)\cos(\omega_j t) \quad (12a)$$

$$A_T^2\left[\sum_{k=K_{\min}}^{K_{\max}} A_k \cos(\omega_k t + \omega_d t)\right]^2 = A_T^2 \sum_{k=K_{\min}}^{K_{\max}} \sum_{\substack{j \\ j\neq k}} A_k^2 \cos^2(\omega_k t + \omega_d t) + 2A_k A_j \cos(\omega_k t + \omega_d t)\cos(\omega_j t + \omega_d t) \quad (12b)$$

$$2A_T \sum_{k=K_{\min}}^{K_{\max}} A_k \cos(\omega_k t) \sum_{j=K_{\min}}^{K_{\max}} A_j \cos(\omega_j t + \omega_d t) = \begin{cases} 2A_T \sum_k A_k^2 \cos(\omega_k t)\cos(\omega_k t + \omega_d t), & \text{if } k = j \\ 2A_T \sum_k \sum_j A_k A_j \cos(\omega_k t)\cos(\omega_j t + \omega_d t), & \text{if } k \neq j \end{cases} \quad (12c)$$

Then, the trigonometric identities are applied to the three equations in (12). As a result, $C_{\mathrm{DVB-T}}(t)$ will be the combination of sinusoidal tones of different frequencies which after further processing as in the diagram of Fig. 1 will be transformed as follows.

1) Constant term to be removed by the last block in the processing chain (dc removal).
2) $\cos(2\omega_k t)$: Cosines with frequency equal to twice each subcarrier are to be removed by the LPF under the condition that $f_{\mathrm{cut-off}} \leq 2 \min_k\{\omega_k\}$.
3) $\cos[(\omega_k + \omega_j)t]$ *and* $cos[(\omega_k - \omega_j)t]$: To understand how these components are processed by the algorithm, two extreme situations must be considered: when $\omega_j = -\omega_k$ and when $\omega_j = \omega_{k+1}$. In the former case, the subcarriers' sum reduces to dc and it is removed as in 1, whereas their difference leads to case 2. In the latter, though the adjacent subcarriers' difference is the minimum possible, further reducing the limitation on the LPF 2 cutoff frequency to $f_{\mathrm{cut-off}} \leq \min_k\{\omega_k - \omega_{k+1}\}$. If this condition is verified, contribution in 2 and 3 are removed by the LPF.
4) $\cos(\omega_d t)$: Which carries the desired Doppler information about the target.

Therefore, since the $f_{\mathrm{cutoff}} \asymp k \cdot 10\,\mathrm{Hz}$, where k is a constant chosen according to the targets' typical speed (usually $k \leq 10$), all undesired components are removed. In fact, the minimum distance between two adjacent subcarriers is $1/T_u \asymp 1$ kHz [9]. Hence, at Point E, after the dc removal, the Doppler signature as in 4) is extracted

$$E_{\mathrm{DVB-T}}(t) \propto \cos(\omega_d t). \quad (13)$$

In (13), the proportionality sign has replaced the equality sign to indicate the fact that the amplitude terms have been omitted at this stage of consideration.

2) *FM Signal:* The generic expression for FM signal [11] of a carrier frequency f_c is

$$s_{\mathrm{FM}}(t) = A\cos(\omega_c t + M(t)) = \Re e\left\{A e^{j\omega_c t} e^{jM(t)}\right\}$$
$$\text{where } M(t) = D_f \int_{-\infty}^{t} m(\tau) d\tau \quad (14)$$

where

A	amplitude of the modulated signal;
$M(t)$	modulating signal;
D_f	modulation index;
$m(\tau)$	modulating message.

Using the same model and symbol notation as in (9), the signal at the receiver input in the case of an FM transmitted signal can be expressed as

$$\begin{aligned} s_{\mathrm{RX-RF}}(t) &= s_{DP}(t) + s_T(t) \\ &= \Re e\left\{e^{j\omega_c t} e^{jM(t)}\left(A_{DP} + A_T e^{j2\pi f_d t}\right)\right\}. \end{aligned} \quad (15)$$

Thus, after downconversion, extraction of the in-phase component and filtering, the resulting signal $A_{\mathrm{FM}}(t)$ is

$$A_{\mathrm{FM}}(t) = A_{\mathrm{DP}}\cos(M(t)) + A_T \cos(M(t) + \omega_d t). \quad (16)$$

At this point, the proposed algorithm extracts the reference signal by applying the hard limiter to (16), hence at Point B, we have $B_{\mathrm{FM}}(t) = \mathrm{sign}(A_{\mathrm{FM}}(t))$. The signal at

Point C is

$$C'_{\mathrm{FM}}(t) = A_{\mathrm{DP}}^2 \cos^2(M(t)) + A_T^2 \cos^2(M(t)+\omega_d) + 2A_{\mathrm{DP}}A_T \cos(M(t))\cos(M(t)+\omega_d) = 1 + \cos(2M(t)) + \cos(2M(t)+2\omega_d t) + \cos(2M(t)+\omega_d t) + \cos(\omega_d t). \quad (17)$$

Then, again, if the second LPF has a cutoff frequency less than twice the lowest modulating signal, i.e., above 50 Hz, the modulation is filtered out and the desired Doppler signature is then extracted after the dc removal

$$E_{\mathrm{FM}}(t) \propto \cos(\omega_d t). \quad (18)$$

REFERENCES

[1] M. Cherniakov
Basic principles of forward-scattering radars
In *Bistatic Radar: Principles and Practice, Part III*. New York, NY, USA: Wiley, 2007.

[2] M. Gashinova, L. Daniel, E. Hoare, V. Sizov, K. Kabakchiev, and M. Cherniakov
Signal characterisation and processing in the forward scatter mode of bistatic passive coherent location systems
EURASIP J. Adv. Signal Process., vol. 2013, no. 1, pp. 1–13, 2013.

[3] M. Cherniakov
Geometry of bistatic radars
In *Bistatic Radar: Principles and Practice, Part II*. New York, NY, USA: Wiley, 2007.

[4] H. Cheng, V. Sizov, M. Antoniou, M. Gashinova, and M. Cherniakov
Optimal signal processing in ground-based forward scatter micro radars
IEEE Trans. Aerosp. Electr. Syst., vol. 48, no. 4, pp. 3006–3026, Oct. 2012.

[5] H. Rohling
100 Years of Radar. Bonn, Germany: Springer, 2004.

[6] N. Willis
Forward-scatter fences
In *Bistatic Radar*. Raleigh, NC, USA: SciTech Publishing, 2005.

[7] M. Gashinova, L. Daniel, M. Cherniakov, P. Lombardo, D. Pastina, and A. De Luca
Multistatic forward scatter radar for accurate motion parameters estimation of low-observable targets
In *Proc. Int. Radar Conf.*, Lille, France, Oct. 13–17, 2014, pp. 1–4.

[8] D. Pastina *et al.*
Target motion estimation via multi-node FSR system
IET Radar, Sonar Navig., vol. 10, no. 1, pp. 3–14, 2016.

[9] ETSI EN 300 744, digital video broadcasting (DVB); framing structure, channel coding and modulation for digital terrestrial television
European Telecommunications Standards Institute, Jan. 2009.

[10] ETSI TS 563, digital audio broadcasting (DAB); transport of advanced audio coding (AAC) audio
European Telecommunications Standards Institute, Jan. 2009.

[11] S. Haykin
Frequency modulation
In *Communication Systems*. New York, NY, USA: Wiley, 2001.

[12] M. Marra, A. De Luca, S. Hristov, L. Daniel, M. Gashinova, and M. Cherniakov
New algorithm for signal detection in passive FSR
in *Proc. IEEE Radar Conf.*, Johannesburg, South Africa, Oct. 27–30, 2015, pp. 218–223.

[13] D. E Hack, L. K. Patton, B. Himed, and M. A. Saville
Detection in passive MIMO radar networks
IEEE Trans. Signal Process., vol. 62, no. 11, pp. 2999–3012, Jun. 1, 2014.

[14] J. J. Spilker
Frequency division multiple access and system nonlinearities
In *Digital Communication by Satellite*. Englewood Cliffs, NJ, USA: Prentice-Hall, 1977.

[15] M. Gashinova, L. Daniel, V. Sizov, E. Hoare, and M. Cherniakov
Phenomenology of doppler forward scatter radar for surface targets observation
Radar, Sonar Navig., IET, vol. 7, no. 4, pp. 422–432, 2013.

[16] N. E. A. Rashid, M. Antoniou, P. Jancovic, V. Sizov, R. Abdullah, and M. Cherniakov
Automatic target classification in a low frequency FSR network
In *Proc. 2008 Eur. Radar Conf.*, Oct. 30–31, 2008, pp. 68–71.

[17] N. Willis
Doppler resolution
In *Bistatic Radar*. Raleigh, NC, USA: SciTech Publishing, 2005.

[18] [Online]. Available: http://www.CST.com. Accessed on: Apr. 2016.

[19] V. Sizov, M. Cherniakov, and M. Antoniou
Forward scattering radar power budget analysis for ground targets
IET Radar Sonar Navig., vol. 1, no. 6, pp. 437–446, 2007.

[20] D. W. O'Hagan, H. Kuschel, M. Ummenhofer, J. Heckenbach, and J. Schell
A multi-frequency hybrid passive radar concept for medium-range air surveillance
IEEE Aerosp. Electron. Sys. Mag, vol. 27, no. 10, pp. 6–15, Oct. 2012.

[21] N. Young, R. Hayward, and D. Dow
Multi-static primary surveillance radar: An air navigation service provider perspective
In *Proc. Int. Radar Symp.*, 2015, pp. 266–271.

[22] [Online]. Available: https://ukfree.tv/transmitters/tv/Sutton_Coldfield/PGSTART2590/. Accessed on: Apr. 2016.

[23] (2015, Nov.). National Instruments Corporation 11500 N Mopac Expy. [Online]. Available: http://www.ni.com/white-paper/52119/en

[24] [Online]. Available: https://flightradar24.com. Accessed on: Apr. 2016.

[25] M. Gashinova, V. Sizov, N. A. Zakaria, and M. Cherniakov
Signal detection in multi-frequency forward scatter radar
In *Proc. 2010 Eur. Radar Conf.*, Sep. 30–Oct. 1, 2010, pp. 276–279.

[26] M. Gashinova, M. Cherniakov, N. A. Zakaria, and V. Sizov
Empirical model of vegetation clutter in forward scatter radar micro sensors
in *Proc. IEEE Radar Conf. 2010*, May 10–14, 2010, pp. 899–904.

[27] [Online]. Available: http://www.advancednavigation.com.au/product/spatial-dual. Accessed on: Apr. 2016.

[28] A. De Luca, M. Contu, S. Hristov, L. Daniel, M. Gashinova, and M. Cherniakov
FSR velocity estimation using spectrogram
In *Proc. 2016 Int. Radar Conf.*, 2016, pp. 1–5.

[29] S. Hristov, L. Daniel, E. Hoare, M. Cherniakov, and M. Gashinova
Target shadow profile reconstruction in ground-based forward scatter radar
in *Proc. 2015 IEEE Radar Conf.*, May 10–15, 2015, pp. 0846–0851.

Micaela Contu was born in Moncalieri, Italy, in 1988. She received the Graduate *cum laude* degree in communication engineering and the Ph.D. degree in radar remote sensing from the University of Rome "La Sapienza," Rome, Italy, in October 2012 and April 2016, respectively.

From December 2015 to May 2016, she was with the Microwave Integrated System Laboratory Group, Birmingham University, Birmingham, U.K. Since June 2016, she has been with VirtuaLabs s.r.l., Rome, as a Radar Engineer. Her main research interests include advanced techniques for bistatic and multistatic radar systems and advanced defense systems.

Alessandro De Luca received the M.Sc. degree in communication engineering from the University of Rome "La Sapienza," Rome, Italy, in 2013. He focused on the study of radar and remote sensing and spent part of his Master's as a Visiting Student with the University of Birmingham, Birmingham, U.K., where since 2014, after a year of working experience, he started his Ph.D. studies at the Microwave Integrated Systems Laboratory.

His main research interests include bistatic and multistatic radar systems and parameter estimation in FSR.

Mr. De Luca received the "Recognition in Young Scientist Contest" for the paper entitled "FSR Velocity Estimation Using Spectrogram" presented at the International Radar Symposium in 2016.

Stanislav Hristov received the B.Sc. degree in physics with particle physics and cosmology from the University of Birmingham, Birmingham, U.K., in 2009, where since September 2009, he has been working toward the Ph.D. degree.

His main research interests include software-defined hardware systems, passive radars, and target imaging and classification in FSR.

Liam Daniel received the M.Sci. degree in theoretical physics from the University of Birmingham, Birmingham, U.K., in 2005, where he also received the Ph.D. degree from the Microwave Integrated Systems Laboratory, School of Engineering, in 2016.

He is currently a Research Fellow with the Microwave Integrated Systems Laboratory, School of Engineering, University of Birmingham. His research interests include bistatic radars with a focus on forward scatter and automotive sensing, both radar and acoustic. Partaking in experimental work, along with accompanying numerical modeling, simulation, and signal processing. His current research focuses on the application of novel low THz radars for automotive applications.

Andy Stove (M'98–SM'04) received the B.A. degree in engineering science and the D. Phil. degree in surface acoustic wave devices from Oxford University, Oxford, U.K, in 1977 and 1981, respectively.

In 1980, he joined Philips Research Laboratories, Redhill, U.K., where he worked on FMCW radar systems with applications in smart ammunition, automotive radar, and low probability of intercept marine navigation. During that period, he was also involved in three bistatic radar projects. In 1996, he joined Racal Radar Defence Systems, which is now a part of Thales, where he worked on the design for the Searchwater 2000 radar family, and on the analysis of the subsequent trials data, including improving the understanding of the behavior of the sea clutter. Other activities have included work on radar target classification and bistatic radar research and acting as an Industry Cochair of the U.K.'s Radar Tower of Excellence. He was also the Cochairman of the NATO SET-184 Noise Radar Group and is currently the Cochairman of its successor group. In 2015, he left Thales, and he is currently with the University of Birmingham, Birmingham, U.K.

Dr. Stove is an Honorary Professor with the University of Birmingham and a Visiting Professor with University College London, London, U.K., and is also a Fellow of the Institution of Engineering and Technology (the successor of the Institution of Electrical Engineers). He has also been an Alan Tayler Visiting Lecturer in applied mathematics with the University of Oxford.

Marina Gashinova received the M.Sc. degree in math from St-Petersburg State University, St-Petersburg, Russia, in 1991, and the Ph.D. degree in physics and math from St-Petersburg Electrotechnical University, St-Petersburg, in 2003.

In 2006, she joined the Microwave Integrated System Laboratory, University of Birmingham, Birmingham, U.K., where she is currently a Senior Lecturer in Radar and RF Sensors, leading the research group on passive and active bistatic radar, THz radar imaging, and automotive sensors. She is an author/coauthor of more than 80 publications in peer-reviewed journals and conferences and a presenter of several invited and focused talks on forward-scatter radar at international conferences, workshops, and seminars.

Mikhail Cherniakov graduated from Moscow Technical University (MTEE), Moscow, Russia, in 1974, with a first-class M.Eng. degree in electronics and received the Ph.D. degree from MTEE in 1980.

At MTEE, he was an Honorary Senior Research Fellow in 1985 and a Doctor of Science (D.Sc) in 1992, then becoming a Full Professor in 1993. In 1994, he was a Visiting Professor with the University of Cambridge, and in 1995, he moved to the University of Queensland, Australia. In 2000, he joined the School of Electronic, Electrical and Systems Engineering, Birmingham, U.K. Here, he founded the Microwave Integrated Systems Laboratory, which is the biggest radar research team in U.K. universities. He is currently a Chair in Aerospace and Electronic Systems, University of Birmingham, Birmingham, U.K., with more than 40 years' experience on R&D in radar systems. He is the author/editor/coauthor of three books, and has more than 250 peer-reviewed publications. His research interests include bistatic and multistatic radar, radars with phased array, automotive, and short-range sensors.

Debora Pastina (M'01) received the Laurea degree in telecommunications engineering and the Ph.D. degree in information and telecommunications engineering from the University of Rome "La Sapienza," Rome, Italy, in 1996 and 2000, respectively.

From July 1998 to March 1999, she carried on research activity with the SAR Processing Team, Defence Evaluation Research Agency, Malvern, U.K. She is currently an Assistant Professor in the DIET Department, University of Rome "La Sapienza," where she teaches different courses in remote sensing and telecommunication. She is involved, and is responsible of, in scientific research projects funded by the Italian Ministry of Research, by the Italian Space Agency, by the European Commission, and by the national radar industry. Her main research interests include SAR/ISAR signal processing, GMTI techniques, clutter models, coherent and incoherent radar detection in non-Gaussian clutter, and CFAR radar techniques. The results of her research activity have been reported in a number of journal and conference papers.

Dr. Pastina was the Chairman of the Local Committee of the IEEE/ISPRS Joint Workshop on Remote Sensing and Data Fusion Over Urban Areas, held in Rome, in November 2001. She was the Publication Chair of the 2008 IEEE Radar Conference, held in Rome, Italy, in May 2008. She has been a Member of the Editorial Board of the *International Journal of Electronics and Communications* (AEÜ, Elsevier) acting as an Area Editor for radar systems and techniques since September 2012. She has served in the technical review committee of many international conferences on radar systems and remote sensing. For many years, she has been a frequent Reviewer for a number of international technical journals.

Pierfrancesco Lombardo (S'93–M'95) received the Laurea degree in electronic engineering and the Ph.D. degree from the University of Rome "La Sapienza," Rome, Italy, in 1991 and 1995, respectively.

In 1991–1992, he served as an Officer Engineer with the Official Test Center, Italian Air Force, Pratica di Mare. In 1994, he was a Research Associate with the University of Birmingham, U.K., while working in the SAR processing team of the Defence Research Agency, Malvern, U.K. During 1995, he was a Research Associate with Syracuse University, New York, USA, working on space-time adaptive processing for AEW and SAR. In June 1996, he joined as an Assistant Professor with the University "La Sapienza," where he was an Associate Professor from 1998 to 2004, and is currently a Full Professor. His main research interests include adaptive radar signal processing, radar clutter modeling, mono- and multichannel coherent radar signal processing, SAR image processing, and radio-location systems. In such areas, he has been a Project Manager of a number of research projects funded by the European Union, by the Italian Space Agency, by the Italian Ministry of Research, and by the Italian radar industry. His research has been reported in more than 200 publications in international technical journals and conferences.

Dr. Lombardo has given tutorial lectures and served in the Technical Committee of many International Conferences on Radar Systems and Signal Processing. He chaired the Technical Committee of the IEEE/ISPRS Workshop on Remote Sensing and Data Fusion Over Urban Areas (URBAN2001), Rome, URBAN2003, Berlin, Germany, URBAN2005, Tempe, AZ, USA, and the IEEE Radar Conference 2008, Rome. He is a corecipient of the BEST PAPER AWARD of the IEEE TRANSACTIONS ON AEROSPACE AND ELECTRONIC SYSTEMS in 2001 and of the BEST PAPER AWARD for the IEEE TRANSACTIONS ON GEOSCIENCE AND REMOTE SENSING in 2003. He is a Member of the IEEE AES Radar System Panel, the Editorial board of the *IET Proceedings on Radar Sonar and Navigation*, and has been an Associate Editor for radar systems for the IEEE TRANSACTIONS ON AEROSPACE AND ELECTRONIC SYSTEMS since June 2001.

Aurora Baruzzi received the Master's degree in telecommunication engineering and the Ph.D. degree from the University of Pisa, Pisa, Italy, in 2011 and 2015, respectively.

She spent six months with the University College London in 2011, working on classification of scaled radar target data collected at ultrasound frequencies. For two years (2012–2014), she was a Research Assistant with the Radar and Surveillance Systems National Laboratory, Pisa, Laboratory of Consorzio Nazionale Interuniversitario per le Telecomunicazioni. Since 2014, she has been in the Passive Radar and Anti-Jamming Techniques Department, Fraunhofer Institute fűr Hochfrequenzphysik und Radartechnik FHR , Wachtberg, Germany. Her research focuses on multisensors multitargets tracking.

Diego Cristallini (M'15) was born in Terni, Italy, in 1981. He received the Graduate *cum laude* degree in telecommunication engineering and the Ph.D. degree in radar remote sensing from the University of Rome "La Sapienza," Rome, Italy, in May 2006 and April 2010, respectively.

From December 2009 to February 2015, he was in the Array-Based Radar Imaging Department, Fraunhofer Institute for High Frequency Physics and Radar Techniques FHR, Wachtberg, Germany. Since March 2015, he has been leading the Team on Passive Covert Radar in the Passive Radar and Anti-Jamming Techniques Department, Fraunhofer FHR, Wachtberg. His research focuses on adaptive multichannel signal processing.

Dr. Cristallini serves as a Reviewer for a number of international technical journals. He received the Best Paper Award at EUSAR 2014.